

Changes of graph structure of transition probability matrices indicate the slowest kinetic relaxations

Teruaki Okushima,^{1,*} Tomoaki Niyama,^{2,†} Kensuke S. Ikeda,^{3,‡} and Yasushi Shimizu^{4,§}

¹College of Engineering, Chubu University, Matsumoto-cho, Kasugai, Aichi 487-8501, Japan

²College of Science and Engineering, Kanazawa University,
Kakuma-cho, Kanazawa, Ishikawa 920-1192, Japan

³College of Science and Engineering, Ritsumeikan University, Noji-Higashi 1-1-1, Kusatsu 525-8577, Japan

⁴Department of Physics, Ritsumeikan University, Noji-Higashi 1-1-1, Kusatsu 525-8577, Japan

(Dated: June 17, 2021)

Graphs of the most probable transitions for a transition probability matrix, $e^{\tau K}$, i.e., the time evolution matrix of the transition rate matrix K over a finite time interval τ , are considered. We study how the graph structures of the most probable transitions change as functions of τ , thereby elucidating that a kinetic threshold τ_g for the graph structures exists. Namely, for $\tau < \tau_g$, the number of connected graph components are constant. In contrast, for $\tau \geq \tau_g$, recombinations of most probable transitions over the connected graph components occur multiple times, which introduce drastic changes into the graph structures. Using an illustrative multi-funnel model, we show that the recombination patterns indicate the existence of the eigenvalues and eigenvectors of slowest relaxation modes quite precisely. We also devise an evaluation formula that enables us to correct the values of eigenvalues with high accuracy from the data of merging processes. We show that the graph-based method is valid for a wide range of kinetic systems with degenerate, as well as non-degenerate, relaxation rates.

I. INTRODUCTION

Complex relaxation dynamics, such as glass dynamics [1–16], folding of biomolecules [17–27], and microcluster dynamics [28–37], are described frequently by kinetic differential equations [38–40]:

$$\frac{d}{dt}\mathbf{p} = K\mathbf{p}, \quad (1)$$

where $\mathbf{p} = (p_1, \dots, p_i, \dots, p_n)$ is the probability distribution vector, and p_i is the probability of being in state i , with n denoting the number of states. K is the transition rate matrix, whose off-diagonal (i, j) element describes the transition rate from the individual state j to the other state i , and whose j th diagonal element is chosen to satisfy $\sum_{i=1}^n (K)_{i,j} = 0$ for each j . Then, the total probability, $\sum_{i=1}^n p_i$, is conserved, and, under a general condition called ergodicity, the eigenvalues, λ_k , of K satisfy the following relation [41]:

$$\lambda_1 = 0 > \lambda_2 \geq \lambda_3 \geq \dots \geq \lambda_n.$$

Moreover, there exist corresponding eigenvectors \mathbf{v}_k such that \mathbf{v}_1 is the equilibrium of the system satisfying $\sum_{i=1}^n (\mathbf{v}_1)_i = 1$, and \mathbf{v}_k ($k = 2, 3, \dots$) are the relaxation modes satisfying $\sum_{i=1}^n (\mathbf{v}_k)_i = 0$.

On the other hand, it is a transition probability matrix $T(\tau)$, describing the time evolution over a finite time in-

terval τ , that is observed experimentally [27]. The mapping of the time evolution is given by

$$\mathbf{p}(t + \tau) = T(\tau)\mathbf{p}(t) \quad (2)$$

for $t = 0, \tau, 2\tau, \dots$, where $T(\tau) = \exp(\tau K)$ holds for the system with the transition rate matrix of K . The eigenvalues of $T(\tau)$ are given by $\bar{\lambda}_k(\tau) = e^{\tau\lambda_k}$ and hence satisfy the following relation [27]:

$$\bar{\lambda}_1(\tau) = 1 > \bar{\lambda}_2(\tau) \geq \bar{\lambda}_3(\tau) \geq \dots \geq \bar{\lambda}_n(\tau) > 0. \quad (3)$$

Note here that τ is regarded as a coarse-graining parameter of time, because any relaxation modes, relaxing with rates faster than $1/\tau$, satisfy $\bar{\lambda}_k(\tau) \sim 0$ and hence are effectively neglected from $T(\tau)$.

Equations (1) and (2) are called the continuous-time and discrete-time Markov state models, respectively. These models have been studied extensively in a wide range of fields. In particular, Markov properties, in which all transitions from an arbitrary state do not depend on any previous states, have been studied in detail because the properties are conditions for satisfying Markov state models. For example, how one can introduce coarse-grained states that ensure the Markov property was studied in [15]. From the τ -dependence of the eigenvalues of $T(\tau)$, the conditions of τ to ensure the Markov properties were elucidated in [18]. In addition to these works, for the renormalization problem, i.e., studies on how to derive lower-dimensional effective Markov state models, a technique with use of the Perron cluster algorithm was invented in [19]. (See, for a review, [27].) Also, we have developed a renormalization method for the Markov state models, where renormalized transition rates between coarse-grained states, called metabasins [42], are defined. We have shown there that the slowest relaxations are obtained accurately with this method [43].

* okushima@isc.chubu.ac.jp

† niyama@se.kanazawa-u.ac.jp

‡ ahoo@ike-dyn.ritsumei.ac.jp

§ shimizu@se.ritsumei.ac.jp

In this paper, by using a multi-funnel model that has been used in our previous studies in Refs. [37, 43], we demonstrate that the metabasin analysis, based upon the most probable path graphs, is successfully applied to the kinetic differential equations of Eq. (1) in Sec. III and the coarse-grained time maps of Eq. (2) in Sec. IV. We then show that these graphs can describe illustratively the characteristics of multi-timescale relaxation dynamics. In particular, a characteristic threshold time τ_g , at which the intra-funnel relaxation dynamics switches to the inter-funnel relaxation dynamics, is definitely extracted. More specifically, we will see that for $\tau < \tau_g$, the metabasins of $T(\tau)$ are composed of almost the same states, in spite of the very frequent intra-metabasin recombinations of most probable transitions. In contrast, for $\tau \geq \tau_g$ the metabasins begin to merge with each other, due to the inter-metabasin recombinations of most probable transitions. We then elucidate in Sec. V A, how and why these graph structure changes correspond to the eigenvalues and the eigenvectors of the slowest relaxation modes. Furthermore, in Sec. V B, we devise an evaluation formula that enables us to correct the values of the eigenvalues with high accuracy from the data of merging processes. As shown in Sec. V C, these graph-based methods are valid for the degenerate, as well as non-degenerate, relaxation rate systems.

In this study, we elucidate how one can extract information about relaxation rates and eigenvectors of K from the graph structures of $T(\tau)$.

II. MODEL

In this section, we introduce the four-funnel model used in Refs. [37, 43], which models basin hopping on high-dimensional potential energy landscapes. We assume that the intra-basin relaxation modes relax so fast that any probability densities $\rho(\mathbf{r})$, where \mathbf{r} is a coordinate vector of all atoms, are expressed as the linear combinations of the intra-basin local equilibria, $\rho_i(\mathbf{r})$, in basins of i . Namely, $\rho(\mathbf{r}) = \sum_{i=1}^n p_i \rho_i(\mathbf{r})$ holds, where n is the number of basins and p_i is the probability of being in basin i . Hence, the probability density $\rho(\mathbf{r})$ is fully specified by the probability vector $\mathbf{p} = (p_1, \dots, p_i, \dots, p_n)$. In addition, the saddle point, which connects basins i and j , is denoted by ij , so that $ij = ji$ holds. Moreover, we assume that the hopping rates between the adjacent basins are given by the Arrhenius transition rates [39, 40]. Namely, the transition rate from state j to state i ($i \neq j$) is given by

$$k_{i,j} = \nu_{i,j} e^{-\beta(E_{ij} - E_j)}, \quad (4)$$

where E_{ij} is the energy of saddle point ij , E_j is the minimum energy in basin j , and $\nu_{i,j}$ is the frequency factor of transition $j \rightarrow i$. In the following, we set $\nu_{i,j} = 1$ for all i and j , for the sake of simplicity.

Figure 1 depicts a four-funnel model in what we call a saddle connectivity graph, where basin energies E_i

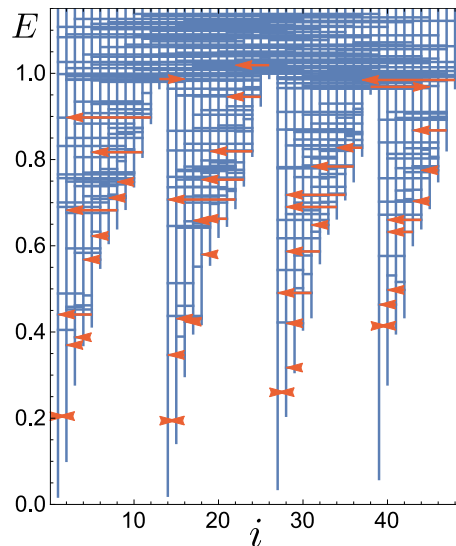


FIG. 1. Saddle connectivity graph for a four-funnel model [37]. Vertical upward lines at $i = 1, 2, \dots, 48$ starting at E_i represent states of i . Horizontal lines at $E = E_{ij}$ connecting i and j represent saddles ij . Most probable transitions $j \rightarrow i$ are also shown by (red) arrows from j to i . (See the text)

and saddle energies E_{ij} are represented for all basins of i and for all saddles of ij , respectively [37]. For the sake of reproducibility, the supplemental materials of LM4funnel.dat and SP4funnel.dat [44] are attached to this paper. E_i is written in the i th line of LM4funnel.dat. The triplet data of i , j , and E_{ij} are written in each line of SP4funnel.dat. Figure 1 shows that metabasins of MB₁, MB₂, MB₃, and MB₄ are composed of $\{1, \dots, 13\}$, $\{14, \dots, 26\}$, $\{27, \dots, 38\}$, and $\{39, \dots, 48\}$, respectively, where the saddles densely connect every state to the other states belonging to the same metabasins as well as the different metabasins. The shapes of metabasins are said to be funnel-like, because, in each metabasin, there exist pathways along which the basin energies E_i and the saddle point energies E_{ij} , respectively, decrease monotonically upon approaching the minimum energy states in the metabasins.

With the use of Eq. (4), we calculated $k_{i,j}$ at $\beta = 5$ and diagonalized matrix K , whose off-diagonal elements are given by $(K)_{i,j} = k_{i,j}$. The eigenvalues of $\lambda_1, \lambda_2, \lambda_3, \lambda_4, \dots$ are given by

$$0, -0.0886, -0.154, -0.235, -1.285, \dots, \quad (5)$$

where $\lambda_1 = 0$ corresponds to the equilibrium, $\lambda_2, \lambda_3, \lambda_4 \sim -0.1$ are the three slowest relaxation rates, and $\lambda_k < -1$ ($k \geq 5$) are the relaxation rates that are more than one order of magnitude faster than the slowest relaxation of λ_2 . In Fig. 2, we show these slowest eigenvectors \mathbf{v}_k for $k = 1, \dots, 4$. We see that the equilibrium distribution \mathbf{v}_1 (circles with dashed lines in Fig. 2) is the superposition of the four intra-metabasin local equilibrium distributions, which have the local maximal probabilities at the funnel bottoms of $i = 1, 14, 27, 39$. Figure 2(a)

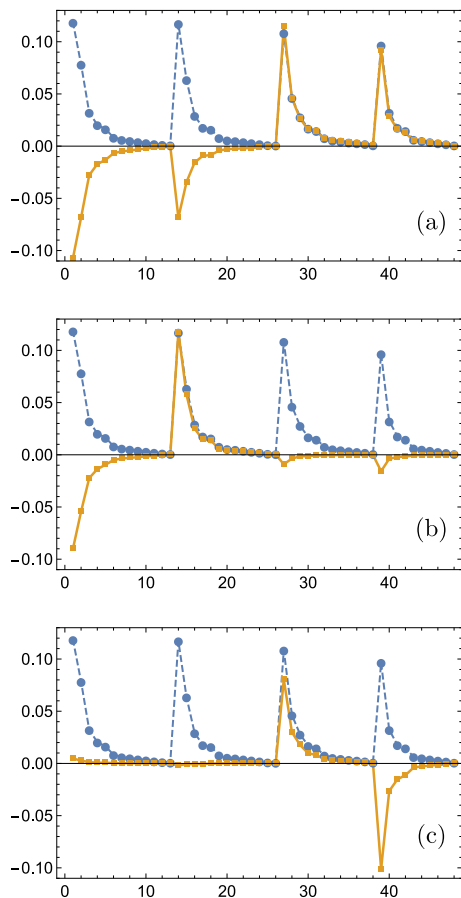


FIG. 2. Eigenvectors \mathbf{v}_2 , \mathbf{v}_3 , and \mathbf{v}_4 of transition rate matrix K for the four-funnel model of Fig. 1 at $\beta = 5$ are plotted in (a), (b), and (c), respectively. In each plot, the equilibrium, \mathbf{v}_1 , is also plotted using circles connected with a dashed line for comparison. Here, \mathbf{v}_1 is normalized as $\sum_{i=1}^n (\mathbf{v}_1)_i = 1$, and \mathbf{v}_k ($k \geq 2$) are scaled such that the components satisfying $(\mathbf{v}_k)_i > 0$ approximately agree with $(\mathbf{v}_1)_i$.

shows that the slowest relaxation mode \mathbf{v}_2 generates the probability flow from the local equilibrium in $\{27, \dots, 48\}$ to the local equilibrium in $\{1, \dots, 26\}$. Similarly, \mathbf{v}_3 generates the probability flow from the local equilibrium in $\{14, \dots, 26\}$ to that in $\{1, \dots, 13\}$ [Fig. 2(b)] and \mathbf{v}_4 generates the probability flow from that in $\{27, \dots, 38\}$ to that in $\{39, \dots, 48\}$ [Fig. 2(c)]. (For details, see the discussion in Sec. IV B.)

Note here that there are various ways of introducing metabasins. For example, Perron cluster algorithms utilize the slowest relaxation eigenvectors of Markov state models [27], and other lumping methods combine states that are separated by small energy barriers [16]. In the following, the metabasins are introduced with the use of the most probable transitions, in the same manner as in [15, 36].

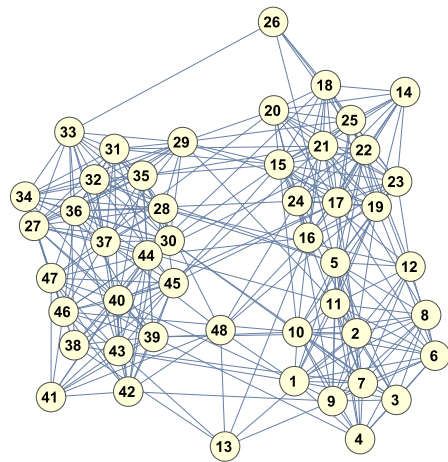


FIG. 3. Transition graph for the four-funnel model of Fig. 1, where all possible transitions between the saddles of ij are represented by the edges connecting vertices i and j .

III. MOST PROBABLE PATH GRAPH OF K

In this section, we discuss why and how we introduce the most probable path graph.

Saddles $ij (= ji)$ enable the transitions of $i \rightarrow j$ and $j \rightarrow i$. Hence, we can draw a graph by connecting the indices of states i and j by edges, for all saddles of ij . Figure 3 shows the transition graph of the four-funnel model depicted in Fig. 1. The graph contains all information about possible transitions or basin adjacencies, except the information about energy levels of E_i and E_{ij} due to the contraction of energy-height information. However, the funnel structures, which are seen in the saddle connectivity graph of Fig. 1, are not apparent in Fig. 3, due to the cumbersome graph structure. The reasons for the failure to capture the funnel features is because the important transitions and the unimportant transitions are equally drawn in Fig. 3.

To tame the graph structural complexity, we here introduce an alternative graph that consists only of the most important transitions. Suppose that the probability vector (p_1, p_2, \dots, p_n) at a moment is given by $p_i = \delta_{i,j}$. Then, any transitions $j \rightarrow i$ can occur at the moment, if $k_{i,j} \neq 0$ ($i \neq j$). Hence, the most probable transition from j is given by $j \rightarrow i$ such that $k_{i,j} = \max\{k_{i',j} \mid 1 \leq i' \leq n, i' \neq j\}$. In Fig. 1, all of the most probable transitions $j \rightarrow i$ are shown by red arrows for the four-funnel model, from which we see that the most probable transitions are folded in the four funnels. This means that the funnel structures can be extracted by the simpler subgraph of the most probable transitions.

In Fig. 4(a), we show the most probable path graph of K , which is the directed graph of most probable transitions for K , where all the most probable transitions j to i are represented by the arrows from j to i . As we expected, the graph is composed of the four connected graph components, which correspond to the four

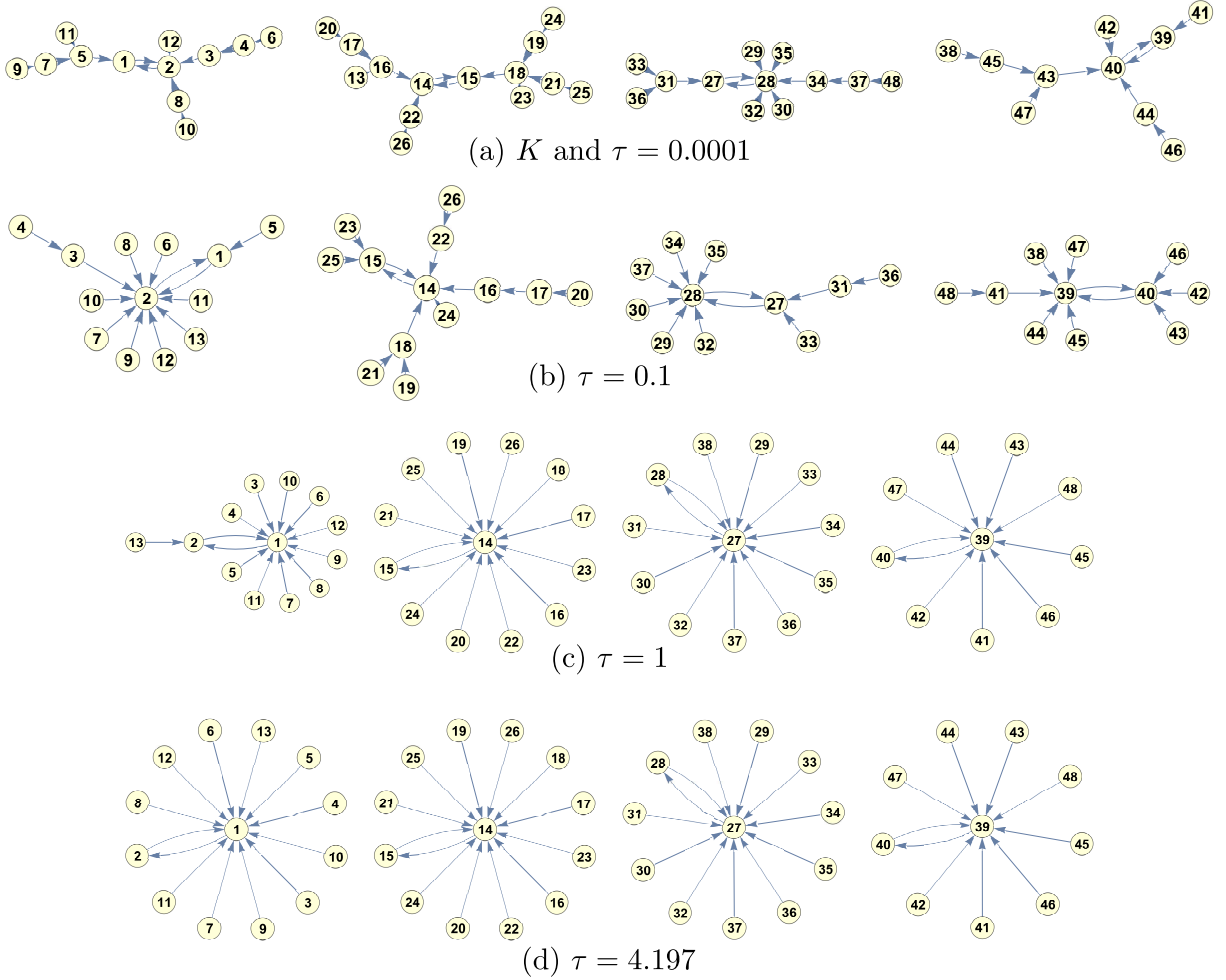


FIG. 4. Most probable path graphs for (a) K and $T(\tau)$ with $\tau = 0.0001$ (both are the same graph) and for $T(\tau)$ with (b) $\tau = 0.1$, (c) $\tau = 1$, (d) $\tau = 4.197$. Each graph of (a)–(d) has four connected graph components, which we call the metabasin. (See the text)

metabasins of MB_1 , MB_2 , MB_3 , and MB_4 depicted by red arrows in Fig. 1. Moreover, we see that each graph component has an attracting cycle $i \rightarrow j \rightarrow i$ (in the following abbreviated as $i \Leftrightarrow j$ for simplicity) containing the lowest energy state in the corresponding metabasin. Hence, we introduce the following compact notation:

$$\begin{aligned}
 MB_1(1 \Leftrightarrow 2) &= \{1, 2, \dots, 12\}, \\
 MB_2(14 \Leftrightarrow 15) &= \{13, 14, \dots, 26\}, \\
 MB_3(27 \Leftrightarrow 28) &= \{27, 28, \dots, 37, 48\}, \\
 MB_4(39 \Leftrightarrow 40) &= \{38, 39, \dots, 47\},
 \end{aligned} \tag{6}$$

where $MB_k(i \Leftrightarrow j) = \{i, j, j', j'', \dots\}$ means that MB_k with cycle $i \Leftrightarrow j$ is composed of $\{i, j, j', j'', \dots\}$.

In this section, we have confirmed that the most probable path graph [Fig. 4(a)], as well as the saddle connectivity graph (Fig. 1), can extract the metabasin structures of transition rate matrices of K .

IV. MOST PROBABLE PATH GRAPH OF $T(\tau)$

Unfortunately, the saddle connectivity graph, as well as other graphing methods, such as the disconnectivity graph [39], is not applicable to the transition probability matrix $T(\tau)$, because both E_j and E_{ij} , which are indispensable for drawing these graphs, are not defined in $T(\tau)$. In contrast, the most probable path graph of $T(\tau)$ is naturally defined, as shown below.

The transition probability from j to i in the duration of time τ is given by $(T(\tau))_{i,j}$. Hence, the most probable transition from j in τ is given by $j \rightarrow i$ such that $(T(\tau))_{i,j} = \max\{(T(\tau))_{i',j} \mid 1 \leq i' \leq n, i' \neq j\}$. The most probable path graph of $T(\tau)$ is drawn by arrows from j to i for all of the most probable transitions $j \rightarrow i$ without difficulty, in the same way as the graph for K was drawn.

In the following, we study the structural changes of the most probable path graph of $T(\tau)$ with varying τ , thereby elucidating that there exists a kinetic threshold,

τ_g , of time interval such that

$$\tau_g \simeq 4.198. \quad (7)$$

Specifically, the members of metabasins are approximately conserved for $\tau < \tau_g$ (Sec. IV A), while there are several mergings of metabasins for $\tau \geq \tau_g$ (Sec. IV B).

Also in Ref. [15], the most probable paths of $T(\tau)$ were studied to investigate the Markov property in metabasin space for a glass former. Moreover, in Ref. [18], the τ -dependencies of $T(\tau)$ were elucidated in order to examine the Markov property in the eigenvector space.

A. $\tau < \tau_g$ case

As shown in Figs. 4(a)–4(d), the most probable path graphs of $T(\tau)$ for $\tau < \tau_g$ have four connected graph components. At $\tau = 0.0001$, the most probable path graphs for $T(\tau)$ and K are identical. Hence, we call the four connected components the metabasins of MB_1 , MB_2 , MB_3 , and MB_4 for $T(\tau)$, as we did for K in Sec. III. Of course, all the cycles and members of MB_k are the same as Eq. (6). Note here that the coincidences of metabasins of K and $T(0.0001)$ means that the metabasin coarse-graining developed in Ref. [43] is a sound basis for the stable description, or the renormalization, of the kinetic evolutions of Eqs. (1) and (2).

The most probable path graph of $T(\tau)$ with $\tau = 0.1$ is shown in Fig. 4(b), where, while all of the cycles are the same as the cycles of $\tau = 0.0001$ in Fig. 4(a), the members of metabasins slightly change: state 13 moves from MB_2 to MB_1 and state 48 moves from MB_3 to MB_4 , which results in

$$\begin{aligned} MB_1(1 \Leftrightarrow 2) &= \{1, 2, \dots, 13\}, \\ MB_2(14 \Leftrightarrow 15) &= \{14, \dots, 26\}, \\ MB_3(27 \Leftrightarrow 28) &= \{27, 28, \dots, 37\}, \\ MB_4(39 \Leftrightarrow 40) &= \{38, 39, \dots, 47, 48\}. \end{aligned} \quad (8)$$

Note here that the moving states of 13 and 48 are the peripheral states that are far from the cycles.

More specifically, the graph of Fig. 4(b) consists of the more direct transitions to the attractive cycles compared to Fig. 4(a). Hence, the longer the time evolution is, the more directly the states arrive at the attractive cycles, which means that the probability vectors from any states tend to evolve into the intra-MB local equilibria to which they belong.

For $1 \leq \tau < \tau_g$, the compositions and the cycles of metabasins do not change as

$$\begin{aligned} MB_1(1 \Leftrightarrow 2) &= \{1, \dots, 13\}, \\ MB_2(14 \Leftrightarrow 15) &= \{14, \dots, 26\}, \\ MB_3(27 \Leftrightarrow 28) &= \{27, \dots, 38\}, \\ MB_4(39 \Leftrightarrow 40) &= \{39, \dots, 48\}. \end{aligned} \quad (9)$$

Note here that these MBs agree with the MBs read from Fig. 1. Moreover, comparing Figs. 4(c) and 4(d), we

see that the most probable transitions are reconnected within MB_1 in the time duration from $\tau = 1$ to $\tau = 4.197$. Especially at $\tau = 4.197$, all transitions become the direct transitions to the most probable states in the intra-metabasin local equilibria, which means that all states within a metabasin evolve to the intra-metabasin local equilibrium in the course of time with $\tau = 4.19$, and, as a result, that all the most probable transitions become the direct transitions to the most probable states in the intra-metabasin local equilibria.

In this subsection, we elucidated the following: (a) The members of metabasins of $T(\tau)$ remain almost unchanged for $\tau < \tau_g$. (b) The cycles of metabasins remain exactly the same. (c) The moving peripheral states that are located far from the attracting cycles can change metabasins to which they belong. (d) At $\tau = 4.19$, all states evolve to the intra-MB local equilibria, and thus the most probable transitions at the time become the direct transitions to the lowest energy states in the metabasins.

B. $\tau \geq \tau_g$ case

For $\tau \geq \tau_g$, the metabasins of $T(\tau)$ merge with each other several times, as shown in Figs. 5(a)–5(e). The merging processes are essentially described by the recombinations of the transitions that are constituents of attractive cycles. As shown in Fig. 4(d), the metabasins at $\tau = 4.197$ ($< \tau_g$) include

$$MB_3(28 \Leftrightarrow 27) \text{ and } MB_4(39 \Leftrightarrow 40). \quad (10)$$

They merge with each other and form a bigger metabasin $MB_{\{3,4\}}$ at $\tau = 4.198$ ($\geq \tau_g$), as

$$MB_{\{3,4\}}(28 \Leftrightarrow 27 \leftarrow 39 \leftarrow 40). \quad (11)$$

Expressions (10) and (11) clearly show that the most probable transition $39 \rightarrow 40$ at $\tau = 4.197$ is changed to $39 \rightarrow 27$ at $\tau = 4.198$. It is this newly created most probable transition that is expected to induce the transport of the excess probability between MB_3 and MB_4 . Let us confirm this expectation by using the eigenvalues and eigenvectors of K . First, $\tau = 4.198$ corresponds to the rate of $-1/\tau \sim -0.24$. At around -0.24 , we indeed find the eigenvalue of $\lambda_4 = -0.235$ from the list (5) of the eigenvalues. The corresponding eigenvector \mathbf{v}_4 is plotted in Fig. 2(c), where the excess ($\mathbf{v}_4 > 0$) and the shortage ($\mathbf{v}_4 < 0$) from the equilibrium distribution, respectively, correspond to the intra- MB_3 and intra- MB_4 local equilibria. Both of these deviations change to zero as $\tau \rightarrow \infty$, since \mathbf{v}_4 evolves as $T(\tau)\mathbf{v}_4 = e^{\lambda_4\tau}\mathbf{v}_4 = e^{-0.235\tau}\mathbf{v}_4 \rightarrow 0$ ($\tau \rightarrow \infty$). Hence, as we expected, the excess probability in the shape of the intra- MB_3 local equilibrium is transported into the intra- MB_4 local equilibrium, by the relaxation mode of \mathbf{v}_4 at around $\tau = \tau_4 = \tau_g = 4.198$.

The next merging of metabasins occurs at $\tau = \tau_3 \equiv 10.35$. Figure 5(b) shows that the graph components of MB_1 and MB_2 remain unchanged from

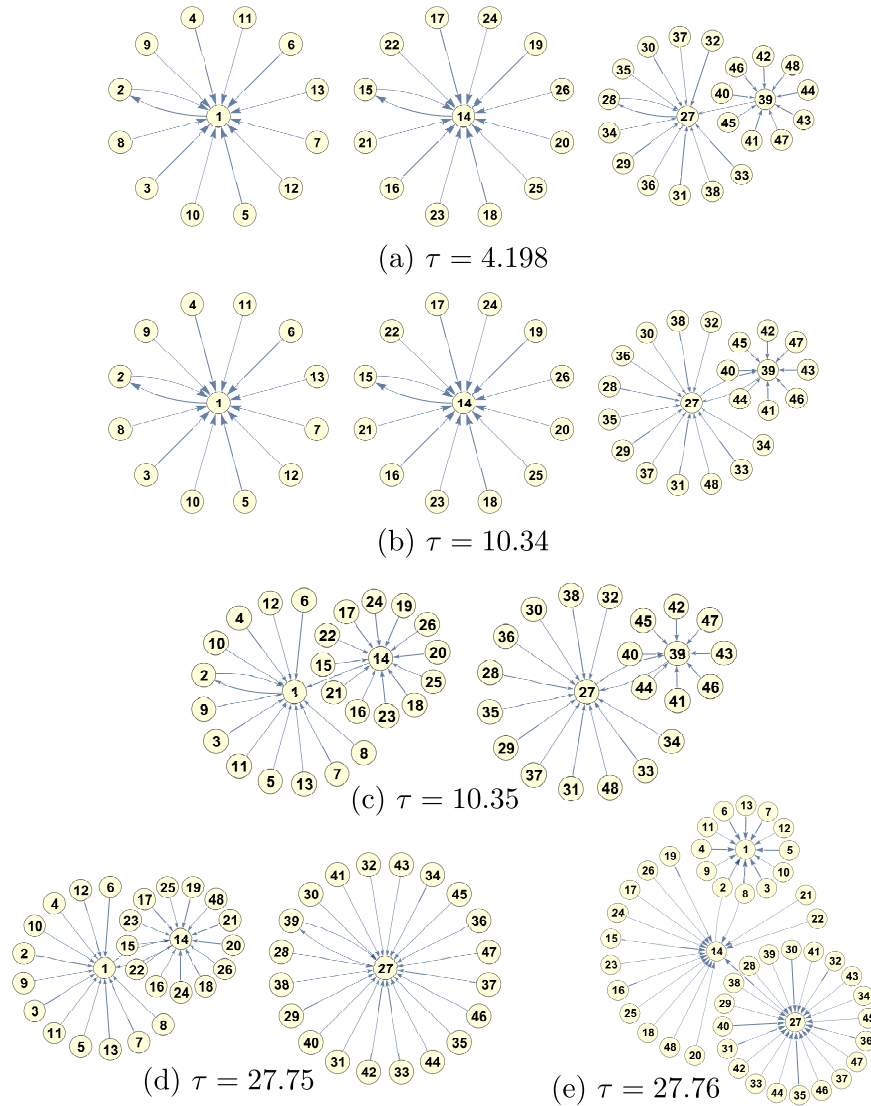


FIG. 5. Most probable path graphs of $T(\tau)$ for (a) $\tau = 4.198$, (b) $\tau = 10.34$, (c) $\tau = 10.35$, (d) $\tau = 27.75$, and (e) $\tau = 27.76$, which show the important recombinations of most probable transitions that lead the merging processes of metabasins.

$\tau = 4.198$ [Fig. 5(a)], while the intra-metabasin structure of $\text{MB}_{\{3,4\}}$ changes from $\text{MB}_{\{3,4\}}(27 \Leftrightarrow 28)$ to $\text{MB}_{\{3,4\}}(27 \Leftrightarrow 39)$, which indicates that the intra- $\text{MB}_{\{3,4\}}$ local equilibrium has been achieved until $\tau = 10.34$. (See the discussion in Sec. V A.) When τ becomes τ_3 , $\text{MB}_1(2 \Leftrightarrow 1)$ and $\text{MB}_2(14 \Leftrightarrow 15)$ merge with each other, and the resulting metabasin is $\text{MB}_{\{1,2\}}(2 \Leftrightarrow 1 \leftarrow 14 \leftarrow 15)$. Again, we consider the eigenvalue and the eigenvector corresponding to this merging process. The eigenvalue that corresponds to the rate of $-1/\tau_3 \sim -0.1$ is identified as $\lambda_3 = -0.154$. We plot the corresponding eigenvector \mathbf{v}_3 in Fig. 2(b), which clearly shows that the excess probability in the shape of the local equilibrium of MB_2 is transported to the local equilibrium of MB_1 , consistently with the graph merging process at $\tau = \tau_3$.

Finally, $\text{MB}_{\{1,2\}}(1 \Leftrightarrow 14)$ and $\text{MB}_{\{3,4\}}(27 \Leftrightarrow 39)$ merge with each other at $\tau = \tau_2 \equiv 27.76$, and the re-

sulting metabasin is given by

$$\text{MB}_{\{\{1,2\},\{3,4\}\}}(1 \Leftrightarrow 14 \leftarrow 27 \leftarrow 39), \quad (12)$$

where we should point out that $\text{MB}_{\{3,4\}}(27 \Leftrightarrow 28)$ and $\text{MB}_{\{1,2\}}(1 \Leftrightarrow 2)$ at $\tau = 4.198$ have changed to $\text{MB}_{\{3,4\}}(27 \Leftrightarrow 39)$ and $\text{MB}_{\{1,2\}}(1 \Leftrightarrow 14)$ until $\tau = 10.35$, respectively. These changes of cycles mean the achievements of local equilibria both in $\text{MB}_{\{1,2\}}$ and in $\text{MB}_{\{3,4\}}$. From this merging process of $\text{MB}_{\{1,2\}}$ and $\text{MB}_{\{3,4\}}$, we again expect the relaxation process between $\text{MB}_{\{1,2\}}$ and $\text{MB}_{\{3,4\}}$ at around $-1/\tau_2 \sim -0.036$. Let us confirm this expectation. The corresponding eigenvalue is $\lambda_2 = -0.0886$, and \mathbf{v}_2 is plotted in Fig. 2(a), which clearly shows that the slowest relaxation mode of \mathbf{v}_2 transports the excess probability in the shape of the intra- $\text{MB}_{\{3,4\}}$ local equilibrium to the intra- $\text{MB}_{\{1,2\}}$ local equilibrium at around the merging time $\tau_2 \sim 20.76$.

C. Summary

Here, we summarize the above findings of how the graph structural changes indicate the properties of the eigenvalues and eigenvectors.

In $\tau < \tau_g$, the most probable transitions are confined in MB_k ($k = 1, 2, 3, 4$). Hence, only intra-metabasin equilibria can be achieved, and the kinetic system remains globally nonequilibrium. In contrast, for $\tau \geq \tau_g$, at around $\tau = \tau_2, \tau_3, \tau_4$ ($\tau_2 > \tau_3 > \tau_4 = \tau_g$) the most probable transitions between metabasins are activated gradually. Especially for larger τ , the kinetic system equilibrates globally via the multiple graph structure changes of the most probable transitions. Based on these findings, we can say that τ_g is a kind of glass-transition time in a sense that within the activation time, the inter-metabasin transitions are effectively prohibited, while at $\tau = \tau_g$ the transitive phase-space volumes become approximately doubled.

V. DISCUSSION

In this section, we show in Sec. V A that the graph structural changes can be interpreted as the manifestation of the time evolution of the local equilibria. In Sec. V B, we show that the discrepancies between merging rates $-1/\tau_i$ and the relaxation rates λ_i arise due to the lag times from the beginnings of the relaxations to the mergings of the basins. Then, we derive a formula for calculating λ_i that corrects the errors arising from the lag times. We also show that, with the formula, one can evaluate the accurate values of λ_i from the actual merging process data. Finally, in Sec. V C, we consider the degenerate λ_i case, where the properties of the slowest relaxation modes are derived similarly to the nondegenerate case, by a graph-based analysis. We confirm that also in this degenerate case, the correcting formula produces accurate estimates of λ_i from the actual merging process data.

A. Intuitive explanation

Here, we show that it can be intuitively understood why the structural changes of the most probable path graphs indicate the existence of the corresponding slowest relaxations. Figure 6 shows the relationship between the most probable transitions from the rightmost states (blue filled curves) and the evolutionary stages of local equilibria from the state. Figure 6(a) describes that the probability distribution evolves into the intra-MB local equilibrium state in a finite time τ_a , which is represented by the red filled curve. Hence, the most probable transition from the rightmost state at that time is the transition to the minimum energy state within MB_4 (curved arrow). Figure 6(b) shows that the probability distribution evolves to the local equilibrium of a wider subsystem

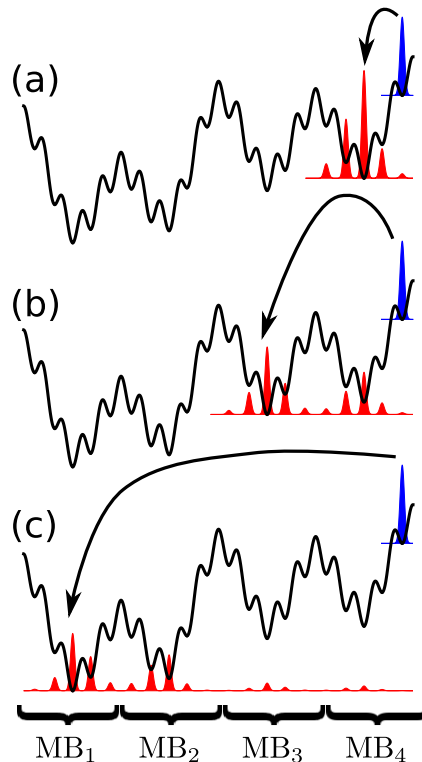


FIG. 6. Schematic illustration of the changes of most probable transitions as a function of τ . Suppose the initial probability distribution is the local equilibrium in the rightmost basin, which is represented by the blue filled bell-shaped curve in each figure. The most probable transitions from the rightmost state at various times of (a) $\tau = \tau_a$, (b) τ_b , and (c) τ_c ($\tau_a < \tau_b < \tau_c$) are indicated by curved arrows.

of $MB_{\{3,4\}}$, at time τ_b . The most probable transition at τ_b is thus from the rightmost state to the minimum energy state in $MB_{\{3,4\}}$ (curved arrow). As a result, the probability flow from MB_4 to MB_3 is generated at $\tau_2 \lesssim \tau_b$, which corresponds to the relaxation mode of rate $\sim -1/\tau_2$ between MB_3 and MB_4 . Further, as depicted in Fig. 6(c), in a global equilibration time of τ_c , the probability distribution evolves to the global equilibrium (red filled curve). The most probable transition at τ_c is, hence, from the rightmost state to the minimum energy state (curved arrow). Hence, the probability flow from $MB_{\{3,4\}}$ to $MB_{\{1,2\}}$ is generated at $\tau_1 \lesssim \tau_c$, which corresponds to the slowest relaxation mode of rate $\sim -1/\tau_1$ between $MB_{\{1,2\}}$ and $MB_{\{3,4\}}$. Here, we have reconfirmed that there exist switches of the most probable transitions from a state, corresponding to changes in the development stages of local equilibria starting from the state. At each switching time of $\tau = \tau_i$ ($i = 1, 2$), the probability flow, which changes the local equilibrium to a wider one, is generated and is related to the slowest relaxations mode with a relaxation rate of $\sim -1/\tau_i$ ($i = 1, 2$). Note that in this illustrating model,

$$\tau_a < \tau_2 < \tau_b < \tau_1 < \tau_c \quad (13)$$

holds. Hence, the glass-transition time τ_g , before which the inter-MB transitions are effectively prohibited, is given by $\tau_g = \min\{\tau_1, \tau_2, \dots\} = \tau_2$.

B. Correction formula for estimation of λ_i

As seen in Sec. IV B, there are small discrepancies between λ_i and $-1/\tau_i$: $\lambda_4 \simeq -1/\tau_4$, $\lambda_3 \lesssim -1/\tau_3$, $\lambda_2 \lesssim -1/\tau_2$. Now, the reason is apparent. The changes of local equilibria, which correspond to the relaxation modes, introduce the change of the most probable paths. Since the relaxation times of $-1/\lambda_i$ are followed by the structural change times τ_i , $-1/\lambda_i < \tau_i$, and equivalently $\lambda_i < -1/\tau_i$, hold. Hence, the discrepancies arise from the lag times from the relaxations to the local equilibrium changes.

The above discussion suggests that we can obtain more accurate estimates of λ_i from the merging process data, by correcting the lag-time errors. Toward that end, we first evaluate the merging time τ , under the condition that an initial local equilibrium distribution \mathbf{p}_a decays to another local equilibrium distribution \mathbf{p}_b by a relaxation mode \mathbf{v} . Since $\mathbf{p}_a - \mathbf{p}_b \propto \mathbf{v}$, the probability distribution at t is given by $\mathbf{p}(t) = \mathbf{p}_b + \exp(\lambda t)(\mathbf{p}_a - \mathbf{p}_b)$. Then, the most probable path from the maximum probability state j_0 of \mathbf{p}_a is $j_0 \rightarrow j_a$ for $t < \tau$, where j_a is the second maximum probability state of \mathbf{p}_a , and it is $j_0 \rightarrow j_b$ for $\tau < t$, where j_b is the maximum probability state of \mathbf{p}_b .

Hence, at the merging time τ , $(\mathbf{p}(\tau))_{j_a} = (\mathbf{p}(\tau))_{j_b}$ holds. By solving this equation for τ , we have

$$\tau = -\frac{1}{\lambda} \log \left(1 + \frac{(\mathbf{p}_a)_{j_a} - (\mathbf{p}_a)_{j_b}}{(\mathbf{p}_b)_{j_b} - (\mathbf{p}_b)_{j_a}} \right), \quad (14)$$

where we see that $\tau > 0$ holds, since $(\mathbf{p}_a)_{j_a} - (\mathbf{p}_a)_{j_b} > 0$, $(\mathbf{p}_b)_{j_b} - (\mathbf{p}_b)_{j_a} > 0$. From Eq. (14), the lag time is given by $\tau + 1/\lambda = -1/\lambda \left\{ \log \left(1 + \frac{(\mathbf{p}_a)_{j_a} - (\mathbf{p}_a)_{j_b}}{(\mathbf{p}_b)_{j_b} - (\mathbf{p}_b)_{j_a}} \right) - 1 \right\}$.

By solving Eq. (14) for λ , we obtain the formula for λ :

$$\lambda = -\frac{1}{\tau} \log \left(1 + \frac{(\mathbf{p}_a)_{j_a} - (\mathbf{p}_a)_{j_b}}{(\mathbf{p}_b)_{j_b} - (\mathbf{p}_b)_{j_a}} \right). \quad (15)$$

Note here that all values on the right-hand side of Eq. (15) are determined by the metabasin-merging process data produced by graph-based analysis.

Let us examine the accuracy of Eq. (15) with the use of the merging process data of K in Sec. IV B. As shown in Sec. IV B, the relaxation mode \mathbf{v}_2 induces a change of the most probable path from $27 \rightarrow 39$ to $27 \rightarrow 14$ at $\tau_2 = 27.76$. With $j_0 = 27$, $j_a = 39$, and $j_b = 14$, $(T(\tau))_{j_a, j_0}$ and $(T(\tau))_{j_b, j_0}$ are plotted as functions of τ in Fig. 7. They surely have an intersection at $\tau = \tau_2 = 27.76$. $(T(\tau))_{j_a, j_0}$ takes the maximum value at $\tau = \tau_a \equiv 11.4$ and decreases monotonically at $\tau > \tau_a$. Hence, τ_a is interpreted as the time required to reach the local equilibrium. Hence, in Eq. (15) we set $\tau = \tau_2 - \tau_a$. Accordingly, we set $(\mathbf{p}_a)_{j_a} =$

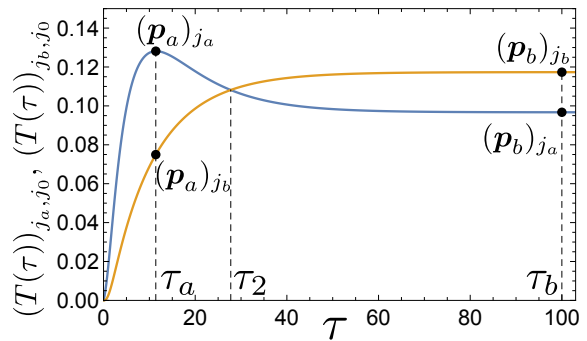


FIG. 7. For the evaluation of λ_2 , $(T(\tau))_{j_a, j_0}$ and $(T(\tau))_{j_b, j_0}$ with $j_0 = 23$, $j_a = 39$, and $j_b = 14$ are plotted by blue and orange lines, respectively, as functions of τ . The intersection at $\tau = \tau_2 = 27.76$ corresponds to the merging process: $\text{MB}_{\{1,2\}}$ and $\text{MB}_{\{3,4\}} \rightarrow \text{MB}_{\{\{1,2\}, \{3,4\}\}}$. The local equilibration time τ_a , $(\mathbf{p}_a)_{j_a}$, $(\mathbf{p}_a)_{j_b}$, $(\mathbf{p}_b)_{j_a}$, and $(\mathbf{p}_b)_{j_b}$, that are necessary for the evaluation of Eq. (15), are shown in this figure.

$(T(\tau_a))_{j_a, j_0} = 0.1281$, $(\mathbf{p}_a)_{j_b} = (T(\tau_a))_{j_b, j_0} = 0.0749$, $(\mathbf{p}_b)_{j_a} = \min\{(T(\tau))_{j_a, j_0} \mid \tau_a < \tau \leq \tau_b\} = 0.0967$, and $(\mathbf{p}_b)_{j_b} = \max\{(T(\tau))_{j_b, j_0} \mid \tau_a < \tau \leq \tau_b\} = 0.1173$ with $\tau_b = 100$, as illustrated in Fig. 7. Under these conditions, we evaluated Eq. (15) and have a result of $\lambda = -0.078$. This is an approximate value of the exact $\lambda_2 = -0.089$, which is much better than the merging rate estimate of $-1/\tau_2 = -0.036$. Note here that, Fig. 7 clearly shows that the relation $\tau_a < \tau_2 < \tau_b$ holds. Namely, we have reconfirmed that Eq. (13) holds for the four-funnel model.

As shown in Table I, we evaluated the values of λ_3 and λ_4 with the use of Eq. (15), from which we see that Eq. (15) generally gives accurate approximations of λ_i . This means that one merging process occurring in the most probable path graph is effectively driven by just one corresponding relaxation mode \mathbf{v}_i for $i = 2, 3, 4$ and further that these merging processes, as well as the relaxation modes, are spatially separated and can be treated to be decoupled from each other.

TABLE I. The i th relaxation rates λ_i , relaxation times $-1/\lambda_i$, merging times τ_i , merging rates $-1/\tau_i$ and the values of Eq. (15), of the four funnel model K . The differences between 2nd and 3rd rows are the lag times.

i	2	3	4
λ_i	-0.089	-0.154	-0.235
$-1/\lambda_i$	11.29	6.49	4.34
τ_i	27.76	10.35	4.20
$-1/\tau_i$	-0.036	-0.0966	-0.238
Eq. (15)	-0.078	-0.165	-0.227

C. Degenerate λ_i cases

We have considered the four-funnel model with the random connectivity between the states, as depicted in Fig. 1. Due to the randomness, this model has nondegenerate eigenvalues of λ_i . However, in particular cases, such as systems with some symmetry, the eigenvalues λ_i can be degenerate. Here, we extend our graph-based arguments to such degenerate λ_i cases.

First, we introduce a degenerate model by modifying the four-funnel model. To this end, recall that the spectral representation of the transition rate matrix K of the four-funnel model is given by

$$K = V\Lambda V^{-1} \quad (16)$$

$$V = [\mathbf{v}_1, \mathbf{v}_2, \mathbf{v}_3, \mathbf{v}_4, \dots], \quad (17)$$

$$\Lambda = \text{diag}(\lambda_1, \lambda_2, \lambda_3, \lambda_4, \dots). \quad (18)$$

Now, we consider the degenerate matrix K' that is obtained by changing the value of λ_4 to the value of λ_3 in K , whose spectral representation is given by

$$K' = V\Lambda'V^{-1} \quad (19)$$

$$\Lambda' = \text{diag}(\lambda_1, \lambda_2, \lambda_3, \lambda_3, \dots). \quad (20)$$

The most probable path graphs of the transition probability matrix $T'(\tau) = \exp(\tau K')$ were examined, where we found the same merging processes as depicted in Fig. 5. However, the merging times τ_i were changed as shown in Table II. From Table II, we see that the doubly degenerate eigenvalues of $\lambda_3 = \lambda_4$ correspond to the resolved merging times $\tau_3 > \tau_4$, which means that lag times, $\tau_i + 1/\lambda_i$, from the relaxation times $-1/\lambda_i$ to the merging times τ_i are different between $i = 3$ and $i = 4$ modes. As shown in Table II, the values of λ_i of K' are estimated with the use of the correcting formula of Eq. (15). Table II clearly shows that the degeneracy of $\lambda_3 = \lambda_4$ is revealed by this estimation.

Assuming here that the system had the same lag times of $i = 3$ and $i = 4$, then $\tau_3 = \tau_4$ would hold and the two merging processes would simultaneously occur

TABLE II. The i th eigenvalues λ_i and the corresponding merging times τ_i ($i = 2, 3, 4$) for the modified four funnel model K' of Eq. (19). K' has the degenerate eigenvalues of $\lambda_3 = \lambda_4 = -0.154$. The lag times $\tau_i + 1/\lambda_i > 0$ are different between $i = 3$ and $i = 4$ modes, although they are in the same eigenspace of $\lambda = -0.154$. Similarly to Table I, the values of λ_i of K' with the use of the correcting formula Eq. (15) were evaluated, where the degeneracy of $i = 3, 4$ is recovered.

i	2	3	4
λ_i	-0.089	-0.154	-0.154
$-1/\lambda_i$	11.29	6.49	6.49
τ_i	27.76	10.35	7.4
$-1/\tau_i$	-0.0360	-0.0966	-0.135
Eq. (15)	-0.0473	-0.165	-0.165

at $\tau = \tau_3$: one was $\text{MB}_1(1 \Leftrightarrow 2)$ and $\text{MB}_2(14 \Leftrightarrow 15) \rightarrow \text{MB}_{\{1,2\}}(2 \Leftrightarrow 1 \leftarrow 14 \leftarrow 15)$, which would induce the probability flow corresponding to the eigenvectors \mathbf{v}_4 , and the other was $\text{MB}_3(27 \Leftrightarrow 28)$ and $\text{MB}_4(39 \Leftrightarrow 40) \rightarrow \text{MB}_{\{3,4\}}(28 \Leftrightarrow 27 \leftarrow 39 \leftarrow 40)$, which would induce the probability flow corresponding to \mathbf{v}_3 . Hence, we were able to extract the relaxation modes $\mathbf{v}_3, \mathbf{v}_4$ by merging graph analysis without any change, in this degenerate lag-time case.

Finally, we consider a triply degenerate matrix K'' , that is obtained by changing the values of λ_4 and λ_3 to the value of $\lambda_2 = -0.089$ in K , whose transition rate matrix is given by

$$K'' = V\Lambda''V^{-1} \quad (21)$$

$$\Lambda'' = \text{diag}(\lambda_1, \lambda_2, \lambda_2, \lambda_2, \dots). \quad (22)$$

The merging times are listed in Table III, which clearly shows that the lag times, $\tau_i + 1/\lambda_i$, are different among $i = 2, 3$ and 4 modes in this triply degenerate case too.

At $\tau_4 = 13.0$, the most probable path from 39 changes from $39 \rightarrow 40$ to $39 \rightarrow 1$, so that MB_1 and MB_4 merged into $\text{MB}_{\{1,4\}}$, which indicates the probability flow from MB_4 to MB_1 . The corresponding relaxation mode $\mathbf{v}'_4 = \mathbf{v}_2 + \mathbf{v}_3 - \mathbf{v}_4$ does exist in the eigenspace of $\lambda = -0.0089$, as shown in Fig. 8(a). At $\tau_3 = 15.4$, the most probable path from 27 changes from $27 \rightarrow 28$ to $27 \rightarrow 1$, so that MB_3 and $\text{MB}_{\{1,4\}}$ next merged into $\text{MB}_{\{\{1,4\},3\}}$. Hence, the probability flow from MB_3 to $\text{MB}_{\{1,4\}}$ is expected. The corresponding relaxation mode $\mathbf{v}'_3 = 1/2\mathbf{v}_2 + 1/2\mathbf{v}_3 + \mathbf{v}_4$ exists in the eigenspace, as shown in Fig. 8(b), from which we see that the excess probability stored in MB_3 is transported into MB_1 and MB_4 by \mathbf{v}'_3 . Lastly, at $\tau_2 = 20.2$, the most probable path from 14 changes from $14 \rightarrow 15$ to $14 \rightarrow 1$, so that MB_2 and $\text{MB}_{\{\{1,4\},3\}}$ merge into $\text{MB}_{\{\{\{1,4\},3\},2\}}$. Hence, the probability flow from MB_2 to MB_1, MB_3 , and MB_4 is expected. The corresponding relaxation mode is $\mathbf{v}'_2 = \mathbf{v}_2 - 2\mathbf{v}_3$, as shown in Fig. 8(c). In short, we have confirmed that in the case of triply degenerate eigenvalues, the three merging processes at $\tau = \tau_4, \tau_3, \tau_2$ exist due to the different lag times. These merging processes

TABLE III. The i th eigenvalues λ_i and the corresponding merging times τ_i ($i = 2, 3, 4$) for the modified four funnel model K'' of Eq. (21). K'' has the degenerate eigenvalues of $\lambda_2 = \lambda_3 = \lambda_4 = -0.089$. The lag times $\tau_i + 1/\lambda_i > 0$ are different among these modes, although they are in the same eigenspace of $\lambda = -0.089$. Similarly to Tables I and II, we estimate the values of λ_i of K'' with Eq. (15), where the degeneracy of $i = 2, 3, 4$ is almost recovered.

i	2	3	4
λ_i	-0.089	-0.089	-0.089
$-1/\lambda_i$	11.29	11.29	11.29
τ_i	20.2	15.4	13.0
$-1/\tau_i$	-0.0769	-0.0649	-0.0495
Eq. (15)	-0.099	-0.103	-0.111

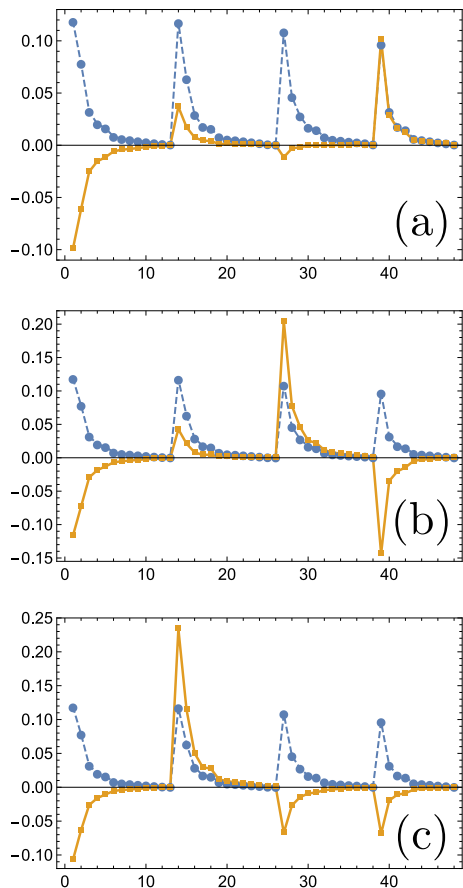


FIG. 8. Eigenvectors of transition rate matrix K'' for the modified four-funnel model of Eq. (21): (a) \mathbf{v}'_4 , (b) \mathbf{v}'_3 , and (c) \mathbf{v}'_2 . In each plot, the equilibrium, \mathbf{v}_1 , is also plotted using circles connected with a dashed line for comparison. Here, \mathbf{v}'_k ($k \geq 2$) are scaled such that the components satisfying $(\mathbf{v}'_k)_i < 0$ approximately agree with $-(\mathbf{v}_1)_i$.

correspond, respectively, to three linearly independent eigenvectors of \mathbf{v}'_4 , \mathbf{v}'_3 , and \mathbf{v}'_2 , in the same eigenspace of λ .

As shown in Table III, the values of λ_i are estimated for K'' , with the use of the correcting formula of Eq. (15). Table III clearly shows that the degeneracy of $i = 2, 3, 4$ is almost reconstructed in the estimated λ_i values. Hence, in this triply degenerate case, each relaxation mode corresponds to each merging process, which enables us to determine the values of λ accurately, with the use of Eq. (15).

Here, assuming again that the three lag times were the same, then, all MBs merged into $\text{MB}_{\{\{\{1,4\},3\},2\}}$ at a certain τ , where the most probable paths simultaneously change from $39 \rightarrow 40$ to $39 \rightarrow 1$, from $27 \rightarrow 28$ to $27 \rightarrow 1$, and from $14 \rightarrow 15$ to $14 \rightarrow 1$. In this case, too, we could extract the three linearly independent eigenvectors of \mathbf{v}'_4 , \mathbf{v}'_3 , and \mathbf{v}'_2 , in the eigenspace of λ , by resolving the accumulating merging into the above three separated mergings. Of course, we might resolve the simultaneous merging into other separated mergings: e.g., MB_1 and

MB_3 merged into $\text{MB}_{\{1,3\}}$; $\text{MB}_{\{1,3\}}$ and MB_2 merged into $\text{MB}_{\{\{1,3\},2\}}$; and $\text{MB}_{\{\{1,3\},2\}}$ and MB_4 merged into $\text{MB}_{\{\{\{1,3\},2\},4\}}$ after that. In this separation, we would obtain another set of linearly independent eigenvectors of \mathbf{v}'_2 , \mathbf{v}'_3 , and \mathbf{v}'_4 , in the same eigenspace of λ .

In summary, we have found the correspondences between the merging processes and the eigenvectors in the case of the eigenspace of λ with multiple degeneracies. A single merging process corresponds to an eigenvector in the eigenspace of λ . Generally, the lag times from the relaxation times $-1/\lambda_i$ to the merging times τ_i vary from eigenvector to eigenvector. Thus, the quasi-degenerate merging rates, $-1/\tau_i$, are resolved. If the lag times are equal, separated reroutings of the most probable paths are postulated in the merging process, from which we can extract the corresponding eigenvectors from the eigenspace of λ . These eigenvectors carry the probability flows induced by the postulated merging processes. Hence, we can extract the eigenvalues and the eigenvectors that correspond to the elemental merging processes, from any degenerate systems, within the error of lag times. Furthermore, with the use of Eq. (15), we can extract the accurate values of λ_i , which are free from the lag-time errors, from the merging process data of degenerate, as well as nondegenerate, λ_i systems.

VI. CONCLUSION

In this paper, we have considered the structural changes of the most probable path graphs of $T(\tau)$. The parameter τ is a coarse-graining parameter in that the modes relaxing faster than $1/\tau$ in rate are neglected from $T(\tau)$. As τ is increased, the most probable path graphs are frequently reconnected, where there exists a specific glass-transition time τ_g , which divides τ into two qualitatively different regions.

For $\tau < \tau_g$, the members of the metabasins (i.e., the connected graph components) remain almost unchanged, and only the intra-metabasin local equilibria can be attained. We have confirmed that not only for transition rate matrices K but also for transition probability matrices $T(\tau)$ the metabasins are suitable bases both for coarse-graining and for renormalization procedures in Ref. [43], since these procedures are not sensitive to the values of τ when $\tau < \tau_g$.

On the other hand, for $\tau \geq \tau_g$, the inter-metabasin reconnections of attracting cycles, which lead to the mergings of metabasins, occur three times. For each value of τ at which metabasins merge with each other, there exists an eigenvalue around the rate of $-1/\tau$, and the corresponding eigenvector clearly shows that the relaxation process corresponds exactly to the merging process of metabasins.

In conclusion, we have revealed that the relaxation properties can be extracted via analyzing structural changes of the most probable path graphs of $T(\tau)$. The advantages of our graph-based method are as follows: (a)

In our method, metabasins are extracted visually directly from the most probable path graphs. In contrast, in the other widely-used methods, such as the Perron cluster algorithm [27], some processing of diagonalizations and linear superpositions is necessary for extracting metabasins. (b) From the merging of metabasins of the most probable path graphs at τ_i , we can evaluate the slowest relaxation rates λ_i as about $-1/\tau_i$ and the corresponding eigenvectors as the probability flows between just merging metabasins. Furthermore, with the use of Eq. (15), which corrects the lag times between $-1/\lambda_i$ and τ_i , one can evaluate the value of λ_i with high accuracy from the merging process. (c) These method developed in this paper are available for a wide range of kinetic systems with degenerate, as well as non-degenerate, relaxation rates.

We remark finally that one can start the metabasin analysis developed in this paper only with the information about the most probable transitions $i \rightarrow j$. The states i and the transition probability matrices $T(\tau)$, required for this analysis, can be estimated by various clustering methods both from simulation datasets and from experimental datasets [20, 27]. Therefore, even if a ki-

netic system was very complicated, it would be relatively easily to extract the information about the most probable transitions and thus the slowest relaxation modes from the transition data via the metabasin analysis. Hence, we hope that this simple graph-based analysis, developed in this work, will be applied to a wide range of realistic kinetic systems for extracting the slowest relaxation modes via experimentally or numerically accessible transition probability matrices.

ACKNOWLEDGMENTS

Y. S. and T. O. are supported by Grant-in-Aid for Challenging Exploratory Research (Grant No. JP15K13539) from the Japan Society for the Promotion of Science. T. O. expresses gratitude to Naoto Sakae and Kiyofumi Okushima for enlightening discussions and continuous encouragement. The authors are very grateful to Shoji Tsuji and Kankikai for the use of their facilities at Kawaraya during this study.

-
- [1] M. Goldstein, *J. Chem. Phys.* **51**, 3728 (1969).
 [2] F. H. Stillinger and T. A. Weber, *Phys. Rev. A* **25**, 978 (1982).
 [3] F. H. Stillinger and T. A. Weber, *Science* **225**, 983 (1984).
 [4] F. H. Stillinger, *Science* **267**, 1935 (1995).
 [5] A. Heuer, *Phys. Rev. Lett.* **78**, 4051 (1997).
 [6] L. Angelani, G. Parisi, G. Ruocco, and G. Vilianni, *Phys. Rev. Lett.* **81**, 4648 (1998).
 [7] P. G. Debenedetti and F. H. Stillinger, *Nature (London)* **410**, 259 (2001).
 [8] S. Sastry, *Nature (London)* **409**, 164 (2001).
 [9] R. A. Denny, D. R. Reichman, and J.-P. Bouchaud, *Phys. Rev. Lett.* **90**, 025503 (2003).
 [10] B. Doliwa and A. Heuer, *Phys. Rev. Lett.* **91**, 235501 (2003).
 [11] B. Doliwa and A. Heuer, *Phys. Rev. E* **67**, 031506 (2003).
 [12] G. A. Appignanesi, J. A. Rodríguez Fris, R. A. Montani, and W. Kob *Phys. Rev. Lett.* **96**, 057801 (2006).
 [13] A. Heuer, *J. Phys. Condens. Matter* **20**, 373101 (2008).
 [14] S. De, B. Schaefer, A. Sadeghi, M. Sicher, D. G. Kanhere, and S. Goedecker, *Phys. Rev. Lett.* **112**, 083401 (2014).
 [15] Y. Yang and B. Chakraborty, *Phys. Rev. E* **80**, 011501 (2009).
 [16] B. Doliwa and A. Heuer, *Phys. Rev. E* **67**, 030501(R), (2003).
 [17] O. M. Becker and M. Karplus, *J. Chem. Phys.* **106**, 1495 (1997).
 [18] N.-V. Buchete and G. Hummer, *J. Phys. Chem. B* **112**, 6057 (2008).
 [19] G. Hummer and Attila Szabo, *J. Phys. Chem. B* **119**, 9029(2015).
 [20] E. Rosta and G. Hummer, *J. Chem. Theory Comput.* **11**, 276 (2015)
 [21] S. S. Cho, Y. Levy, and P. G. Wolynes, *Proc. Natl. Acad. Sci. U. S. A.* **103**, 586 (2006).
 [22] G. R. Bowman and V. S. Pande, *Proc. Natl. Acad. Sci. U. S. A.* **107**, 10890 (2010).
 [23] J. Wang, R.J. Oliveira, X. Chu, P. C. Whitford, J. Chahine, W. Han, E. Wang, J. N. Onuchic, and V.B.P. Leite, *Proc. Natl. Acad. Sci. U. S. A.* **109**, 15763 (2012).
 [24] D. Shukla, C.X.Hernández, J.K. Weber, and V. S. Pande, *Acc. Chem. Res.* **48**, 414 (2015).
 [25] F. Pontiggia, D.V. Pachov, M.W. Clarkson, J. Villali, M.F. Hagan, V.S. Pande, and D. Kern, *Nat. Commun.* **6**, 7284 (2015).
 [26] B. Zhang, W. Zheng, G.A. Papoian, and P.G. Wolynes, *J. Am. Chem. Soc.* **138**, 8126 (2016).
 [27] *An Introduction to Markov State Models and Their Application to Long Timescale Molecular Simulation*, edited by G. R. Bowman, V. S. Pande, and F. Noé (Springer, New York, 2013).
 [28] G. A. Breaux, R. C. Benirschke, T. Sugai, B. S. Kinnear, and M. F. Jarrold, *Phys. Rev. Lett.* **91**, 215508 (2003).
 [29] H. Haberland, T. Hippler, J. Donges, O. Kostko, M. Schmidt, and B. von Issendorff *Phys. Rev. Lett.* **94**, 035701 (2005).
 [30] K. Joshi, S. Krishnamurty, and D. G. Kanhere, *Phys. Rev. Lett.* **96**, 135703 (2006).
 [31] C. Hock, S. Straßburg, H. Haberland, B. v. Issendorff, A. Aguado, and M. Schmidt, *Phys. Rev. Lett.* **101**, 023401 (2008).
 [32] C. Hock, C. Bartels, S. Straßburg, M. Schmidt, H. Haberland, B. von Issendorff, and A. Aguado *Phys. Rev. Lett.* **102**, 043401 (2009).
 [33] Y. Kimura, Y. Saito, T. Nakada, and C. Kaito, *Physica E* **13**, 11 (2002).
 [34] T. Niiyama, S.-I. Sawada, K. S. Ikeda, and Y. Shimizu, *Eur. Phys. J. D* **68**, 1 (2014).
 [35] T. Niiyama, T. Okushima, K. S. Ikeda, and Y. Shimizu,

- Chem. Phys. Lett. **654**, 52 (2016).
- [36] T. Okushima, T. Niiyama, K. S. Ikeda, and Y. Shimizu, Phys. Rev. E **76**, 036109 (2007).
- [37] T. Okushima, T. Niiyama, K. S. Ikeda, and Y. Shimizu, Phys. Rev. E **80**, 036112 (2009).
- [38] C. L. Brooks III, J.N. Onuchic, D.J. Wales, Science **293**, 612(2001).
- [39] D. J. Wales, *Energy Landscapes: Applications to Clusters, Biomolecules and Glasses* (Cambridge University Press, Cambridge, UK; New York, 2003).
- [40] F. H. Stillinger, *Energy Landscapes, Inherent Structures, and Condensed-Matter Phenomena* (Princeton University Press, Princeton, New Jersey, 2016).
- [41] H. Haken, *Synergetics, An Introduction: Nonequilibrium Phase Transitions and Self-Organization in Physics, Chemistry, and Biology*, 3rd rev. enl. ed. (Springer, Berlin; New York, 1983).
- [42] For another formulation of metabasin decompositions: See K. Klemm, C. Flamm, and P. F. Stadler, Eur. Phys. J. B **63**, 387 (2008).
- [43] T. Okushima, T. Niiyama, K.S. Ikeda, and Y. Shimizu, Phys. Rev. E **97**, 021301(R) (2018).
- [44] See Ancillary files for the local minimum dataset of the four-funnel model, and for the saddle point dataset of the four-funnel model.